Supporting Information for

Rounded layering transitions on the surface of ice

by

Pablo Llombart[†,‡], Eva G. Noya[‡], David N. Sibley[§], Andrew J. Archer[§] and Luis G. MacDowell[†]

[†]Departamento de Química-Física (Unidad de I+D+i Asociada al CSIC), Facultad de Ciencias Químicas, Universidad Complutense de Madrid, 28040 Madrid, Spain,

[‡]Instituto de Química Física Rocasolano, CSIC, Calle Serrano 119, 28006 Madrid, Spain and

[§]Department of Mathematical Sciences, Loughborough University, Loughborough LE11 3TU, United Kingdom.

RESULTS FOR THE PRIMARY PRISM FACET

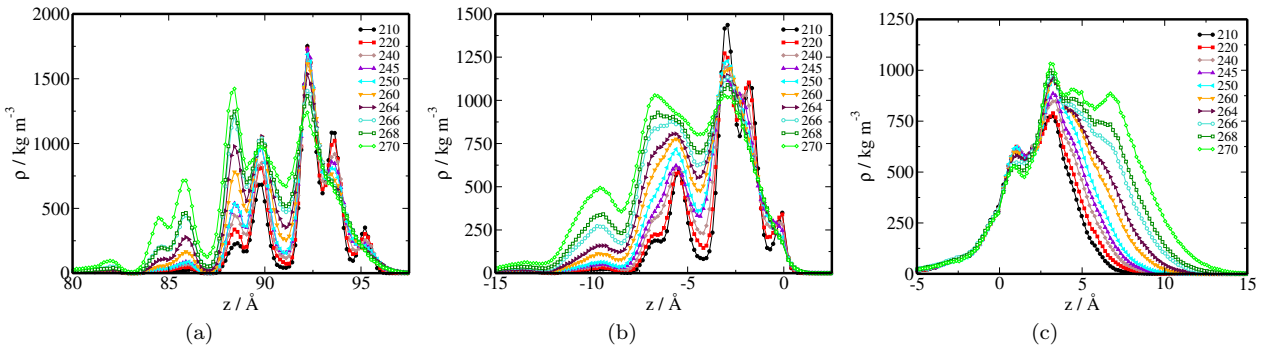

FIG. 1. Density profiles of liquid-like molecules for the primary prism interface as measured relative to (a) the laboratory reference frame (b) the f-v surface and (c) the i-f surface.

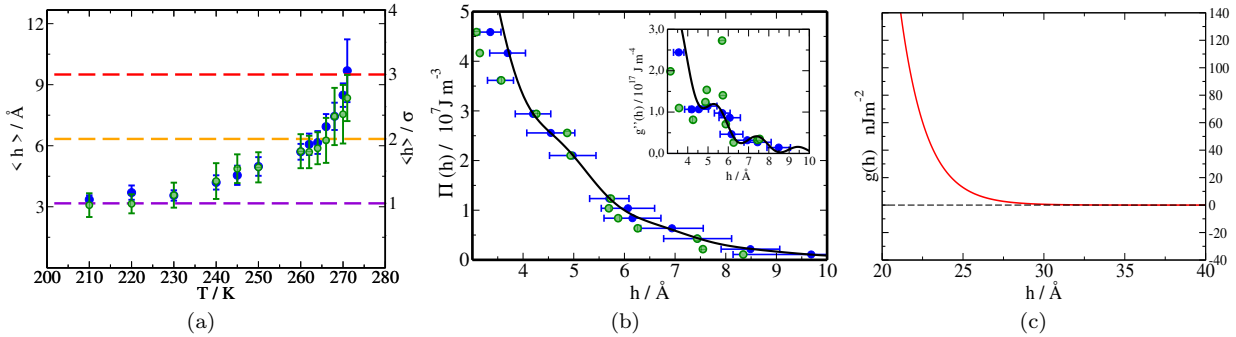

FIG. 2. Film thickness (a), disjoining pressure (b), and interface potential (c) for the primary prism facet. Results are shown for two system sizes with $n_x \times n_y = 5120$ (blue filled circles) and $n_x \times n_y = 1280$ (green hollow circles) molecules. (a) The dashed lines indicate discrete film heights in units of the molecular diameter. (b) The lines are a fit to Eq. (2). The insets show inverse surface susceptibilities as obtained from numerical derivatives (symbols) and from analytical derivatives of the fits (lines). Error bars here are shown only for the data fitted to Eq. (2). Panel (c) shows the decay of the interface potential at intermediate distances as extrapolated from the fit to Eq. (2). The decay of the interface potential here is monotonic.

DISJOINING PRESSURE

The three phases involved are the ice substrate (i), the water film (f) and the vapor (v). The discussion below is rather general, so here we refer to the three phases as solid (s), liquid (l) and vapor (v). Consider an inert substrate in

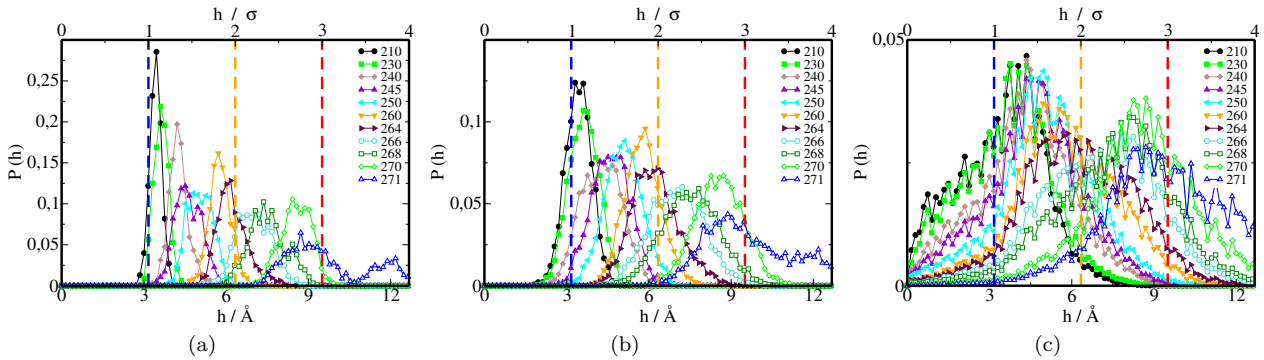

FIG. 3. System size analysis of thickness distributions at the primary prism plane. Panels (a) probability distribution of the global film thickness, h. (b) probability distribution of the partial film thickness $h_{1/4}$. (c) probability distribution of the local order parameter $h(\mathbf{x})$. Dashed vertical lines show the film thickness in units of the molecular diameter. Results are shown for temperatures in the range from T=210 K to T=271 K, with color code as indicated on the figure.

contact with a stable vapor phase at fixed temperature, T. It is convenient to study the system in the grand canonical ensemble, where the chemical potential μ is fixed at the outset, and one assumes the adsorbed layer can grow to its equilibrium value while the vapor pressure remains constant. By this device, one fixes the vapor pressure of the system to the corresponding bulk vapor pressure $p_v(T,\mu)$ at the selected chemical potential. The corresponding bulk liquid phase of equal temperature and chemical potential has a bulk pressure, $p_l(T,\mu)$.

Consider that (T,μ) are such that the bulk vapor phase is more stable than the bulk liquid phase. For a column of height h filled by bulk vapor, the free energy per unit surface is given by $\omega_v(T,\mu) = -p_v(T,\mu)h$. Similarly, for an equivalent column filled with bulk liquid, the corresponding free energy is given as $\omega_v(T,\mu) = -p_l(T,\mu)h$. Below the bulk liquid-vapor coexistence, it always holds $p_v(T,\mu) > p_l(T,\mu)$, such that the vapor phase has the lowest free energy and is the preferred phase. The free energy difference per unit surface area between a liquid filled and vapor filled column is given as $\Delta\omega(T,\mu) = \Delta p_{lv}(T,\mu)h$, where $\Delta p_{lv}(\mu,T) = -[p_l(T,\mu) - p_v(T,\mu)]$ is the familiar Laplace pressure difference used in classical nucleation theory.

If the column of bulk phase is moved next to the substrate, however, a finite amount of liquid phase is usually stabilized, even if the thermodynamic fields have been selected such that the bulk vapor phase is most stable. The interface potential, $g(h)$ accounts for the free energy gained by the liquid phase in contact with the substrate.

The excess free energy of the liquid film of thickness h adsorbed on a substrate is given as:

$$\omega(h;T,\mu) = \gamma_{sl} + \gamma_{lv} + g(h;T) - \Delta p_{lv}(T,\mu)h, \tag{3}$$

Here, $-\Delta p(T,\mu)h$, is the bulk free energy cost to replace the bulk vapor by a liquid film, $g(h)$ accounts for the free energy gained by the bulk liquid phase due to the influence of the substrate at liquid-vapor coexistence, while γ_{sl} and γ_{lv} are the solid-liquid and liquid-vapor interfacial tensions, respectively.

The condition of equilibrium for the adsorbed film at constant T,μ is:

$$\frac{d\omega(h;T,\mu)}{dh} = 0. \tag{4}$$

This provides the celebrated Derjaguin equation [45–47]:

$$\Pi(h;T) = -\Delta p_{lv}(T,\mu), \tag{5}$$

where $\Pi(h;T)$ is the disjoining pressure, defined as $\Pi(h;T) = -dg(h;T)/dh$.

In standard applications for adsorbed liquids on an inert substrate, one usually measures an adsorption isotherm, i.e., $h = h(T,\mu)$, at fixed temperature, while changing the chemical potential (or vapor pressure). The disjoining pressure is calculated by matching the measured equilibrium film thickness at increasing vapor pressure with the corresponding pressure difference, $\Delta p_{lv}(T,\mu)$ [47].

For a premelting film, the situation is far more complicated, because adsorption from the vapor phase takes place on a solid substrate that is found at phase coexistence with the vapor. i.e., the vapor-substrate equilibrium states only exist along the sublimation or solid-vapor coexistence line, corresponding to a fixed chemical potential $\mu_{sv} = \mu_{sv}(T)$.

Therefore, at fixed temperature one cannot meaningfully collect equilibrium film thicknesses h as a function of vapor pressure, since equilibrium is achieved only at exactly the solid-vapor coexistence pressure, $p_{sv}(T, \mu_{sv}(T))$.

The way out is to relax the constraint of fixed temperature. Instead, we collect the equilibrium film thicknesses $h(T)|_{sv} = h(T, \mu_{sv})$ along the sublimation line, where the notation $X(T)|_{sv}$ denotes a property $X(T)$ measured at the chemical potential $\mu_{sv} = \mu_{sv}(T)$ of solid/vapor coexistence. These film thicknesses are then mapped onto $\Delta p_{lv}(T)|_{sv}$, i.e., the pressure difference between bulk liquid and vapor phases measured at the solid-vapor coexistence chemical potential.

Taking into account that the temperature dependence of $g(h;T)$ and $\Pi(h;T)$ is small, one can get a single disjoining pressure master curve $\Pi(h)$ from these data. Accordingly, the function $\Pi(h)$ is obtained in three steps:

- Measure the equilibrium film thickness $h(T)|_{sv}$ along the sublimation line. In practice, this is readily done by direct coexistence NVT simulations. Placing a slab of ice in contact with vacuum at a temperature T, the system gradually equilibrates and attains solid-vapor coexistence. Accordingly, once the system is well equilibrated, the vapor phase is automatically selected to exhibit the sublimation vapor pressure without a priori knowledge of the corresponding chemical potential. In between the almost empty vapor phase and the bulk ice phase, a premelting liquid film is formed in a few nanoseconds. The equilibrium film thickness that is obtained corresponds to the desired curve, $h(T)|_{sv}$.

- Calculate the Laplace pressure difference between bulk liquid and vapor phases at the solid-vapor coexistence chemical potential, $\Delta p_{lv}(T)|_{sv}$. Below we show that this pressure difference can be related to the liquid-vapor and solid-vapor coexistence pressures. Using the Clapeyron equation the coexistence pressures may be obtained from triple point data only. In practice, we assume an ideal gas for the vapor phase, and obtain accurate approximations for the solid and liquid properties at the triple point from NpT simulations at zero pressure (see below).

- Map the results of $h(T)|_{sv}$ onto $\Delta p_{lv}(T)|_{sv}$ to obtain the disjoining pressure curve from Eq. (5) as:

$$\Pi(h(T)|_{sv}) = -\Delta p_{lv}(T)|_{sv} \tag{6}$$

LAPLACE PRESSURE DIFFERENCE ALONG THE SUBLIMATION LINE

In order to evaluate the disjoining pressure, we need to know the Laplace pressure difference $\Delta p_{lv}(T)|_{sv}$ between the bulk liquid and vapor phases at equal temperature and chemical potential, for selected chemical potentials along the sublimation line.

It turns out that this calculation can be performed following thermodynamic calculations that are familiar in classical nucleation theory.

Here, we are interested in calculating the pressure difference $\Delta p_{lv}(T) = p_l(T, \mu) - p_v(T, \mu)$ between an adsorbed liquid phase and a reservoir vapor phase with chemical potential μ. Using the Gibbs-Duhem equation, $dp = \rho\, d\mu$, with ρ, the bulk density, we write:

$$d(p_l - p_v) = (\rho_l - \rho_v) d\mu. \tag{7}$$

Since the vapor density is much smaller than the liquid density, we assume $\rho_l - \rho_v \approx \rho_l$. Furthermore, since the liquid is effectively incompressible for the small chemical potential changes that concern us here, we assume constant liquid density and integrate the above equation from the liquid-vapor coexistence chemical potential to arbitrary chemical potential at fixed temperature, yielding:

$$p_l(T, \mu) - p_v(T, \mu) = \rho_l(\mu - \mu_{lv}), \tag{8}$$

where μ_{lv} is the chemical potential at liquid-vapor coexistence and we have taken into account that $p_l(T, \mu_{lv}) - p_v(T, \mu_{lv}) = 0$.

Now, assuming the vapor phase is an ideal gas, we obtain:

$$p_l(T, \mu) - p_v(T, \mu) = \rho_l RT \ln p/p_{lv}(T), \tag{9}$$

where $p(T)_{lv}$ is the liquid-vapor coexistence pressure and p is the pressure of the vapor phase with arbitrary chemical potential μ. This is the result used in classical nucleation theory for the pressure difference of a liquid nucleus in

equilibrium with the vapor reservoir phase. Here we use the same equation for the adsorbed liquid layer in equilibrium with a vapor reservoir phase.

It follows immediately that the sought Laplace pressure difference along the sublimation line, where $p = p_{sv}$ by definition, is given as:

$$\Delta p_{lv}|_{sv} = \rho_l RT \ln \frac{p_{sv}(T)}{p_{lv}(T)}. \tag{10}$$

Therefore, $\Delta p_{lv}(T)|_{sv}$ may be calculated from knowledge of the vapor pressures along the condensation and sublimation lines.

In order to obtain $p_{sv}(T)$ and $p_{lv}(T)$, we invoke the Clausius equation for the coexistence pressure, $p_{\alpha v}$ of an arbitrary phase, α, with the bulk vapor:

$$\frac{dp_{\alpha v}}{dT} = \frac{\Delta H_{\alpha v}}{T \Delta V_{\alpha v}}, \tag{11}$$

where $\Delta H_{\alpha v}$ and $\Delta V_{\alpha v}$ are the enthalpy and volume change of transition. For water below the triple point, the volume of the vapor phase is more than 1000 times larger than that of either liquid or solid phases, so we can approximate $\Delta V_{\alpha v}$ to the volume of the vapor phase V_v, and further replace this with the ideal gas equation, leading to the Clausius-Clapeyron result:

$$\frac{dp_{\alpha v}}{p} = \frac{\Delta H_{\alpha v}}{RT^2} dT. \tag{12}$$

In many applications, this equation is integrated under the assumption of constant $\Delta H_{\alpha v}$. We improve this approximation by expanding the enthalpy of phase change to first order about the triple point:

$$\Delta H = \Delta H_t + \Delta C_{p,t}(T - T_t), \tag{13}$$

where $\Delta C_{p,t}$ is the difference of heat capacities between the corresponding condensed phase and the coexisting vapor phase at the triple point. This then finally yields:

$$\ln(p_{\alpha v}(T)/p_t) = \frac{\Delta H_t - \Delta C_{p,t} T_t}{R} \left[1/T_t - 1/T\right] + \frac{\Delta C_{p,t}}{R} \ln(T/T_t), \tag{14}$$

where here ΔH_t is the enthalpy of phase change, and the subindex α corresponds to either liquid or solid phases.

In order to evaluate this equation, we calculated enthalpies and heat capacities for the TIP4P/Ice model at the triple point temperature $T_t = 272$ K and zero pressure. Results for the required properties may be found in Table I.

H_t^{iv} / KJ mol^{-1}	H_t^{wv} / KJ mol^{-1}	$C_{p,t}^{i}$/ J mol^{-1}K^{-1}	$C_{p,t}^{w}$ / J mol^{-1}K^{-1}
-61.03	-55.64	65.60	107.26

TABLE I. Thermophysical properties of the TIP4P/Ice model at the triple point $T_t = 272$ K, required for the determination of the sublimation and condensation pressures.

MOMENTS OF THE DISTRIBUTIONS AND ROUNDED TRANSITIONS

Since the probability distributions of the order parameter in Fig. 3 of the main manuscript and Fig. 3 of the supplementary material are normalized to unity, a rough estimate of the mean squared amplitude of the fluctuations can be made from the height of the maxima of the distributions. From these plots, one finds that the maxima corresponding to partially filled layers are less pronounced than those corresponding to filled layers. Accordingly, the fluctuations are larger for the former and we can estimate the loci of the rounded transitions from the distribution with largest fluctuations. By visual inspection, this suggests rounded transitions at about 235 K and 266 K for the basal face, and at about 250 K and 266 K for the prism face. Of course, because of the limited statistics, the finite size transitions are given with an error of ± 2 K at least.

A quantitative analysis requires consideration of the probability distribution in more detail. In our simulations, the system is found at solid vapor coexistence by construction. The chemical potential is therefore fixed exactly at

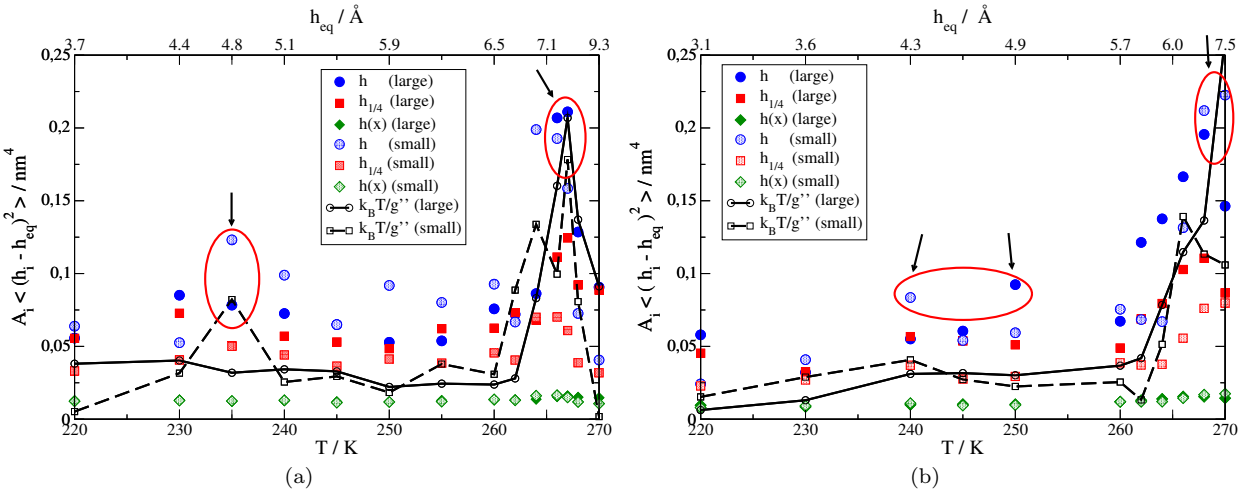

FIG. 4. Scaled mean squared fluctuations of the film thickness. Results are shown for the large (filled symbols) and small (hollow symbols) systems. The latter is 2×2 smaller than the former. The figure shows moments for fluctuations of the global film thickness, h (circles), for subsystems with size 1/4, $h_{1/4}$ (squares) and for the local thickness $h(x)$ (diamonds). Black lines show the scaled mean squared fluctuations as given by the right hand side of Eq. (17), with $\chi_{\parallel}^{-1}$ estimated from the second derivatives of the interface potential, $g''(h)$. Results are shown for large (full lines) and small (dashed lines) systems. Arrows point roughly to the location of the maxima of mean squared fluctuations.

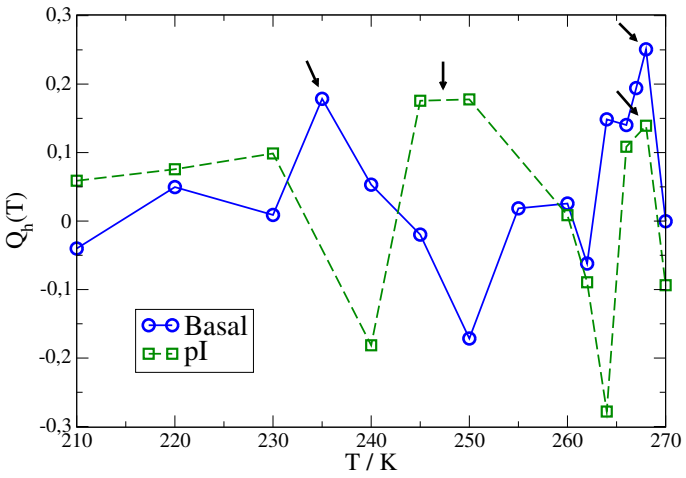

FIG. 5. Binder cumulants of the global order parameter for the large (blue circles) and small (green squares) systems. The arrows point to maxima of the cumulants, which serves to roughly locate the transitions.

coexistence. Furthermore, the system features a large bulk phase, which roughly serves as a particle and heat reservoir for the premelting film. Therefore, we may consider the premelting film as effective being treated grand canonically. For a system away from the line of layering transitions, the surface free energy in Eq. (3) at the imposed constant temperature and chemical potential can be expanded to quadratic order as:

$$\omega(h;T,\mu) = \omega(h_{eq},T,\mu) + \frac{1}{2}\chi_{\parallel}^{-1}(h-h_{eq})^2, \tag{15}$$

where h_{eq} is the equilibrium film thickness, and the susceptibility has been defined as $\chi_{\parallel}^{-1} = g''(h_{eq})$. The surface free energy is related to the probability distribution as $A\omega(h;T,\mu) = -k_BT \ln P(h;T,\mu)$, where A is the lateral area. Accordingly, the probability distribution of the order parameter is (c.f. Ref.[54, 55]):

$$P(h) = Ce^{-\frac{1}{2}\beta A\chi_{\parallel}^{-1}(h-h_{eq})^2}, \tag{16}$$

with C a normalization constant. This has a Gaussian form, so the mean squared fluctuations of h in a system with

lateral size A will obey:

$$A\langle(h - h_{eq})^2\rangle = k_B T/\chi_{\parallel}^{-1}. \tag{17}$$

Fig. 4 shows the scaled mean squared fluctuations, which, from Eq. (17), should become constant, independent of the system size in the thermodynamic limit for non-singular transitions. From the figure we find this holds indeed already for the limited system sizes studied here. Despite a considerable scatter of the simulation data, maxima of the fluctuations for a fixed system size are observed roughly as estimated from visual inspection of the distributions. As an additional consistency check, we also show as a black line the expectation for the scaled mean squared fluctuations as obtained from the inverse susceptibilities of the interface potential depicted in the inset of Fig. 2(b) of the main manuscript and this document. The agreement seems fairly good, considering the limited statistics and finite size effects.

In order to further analyse the rounded transitions, it is convenient to consider the Binder cumulant of the distributions, which is given as [55]:

$$Q_h = 1 - \frac{1}{3}\frac{\langle(h - h_{eq})^4\rangle}{\langle(h - h_{eq})^2\rangle^2}. \tag{18}$$

For a system away from a critical point, the distributions are Gaussian, and Q_h is approximately zero. Close to a phase transition, however, Q_h is expected to approach $2/3$ in the thermodynamic limit.

Fig. 5 shows plots of Q_h as obtained from the moments of the global order parameter of the largest system. Results for the remaining order parameters are similar, but are quite noisy and do not afford a study of system size effects. From the plot, it can be clearly seen that most values of Q_h fluctuate about 0, the result expected for a disordered phase. The location of rounded transitions is visible in the maxima of the cumulants, as indicated by the arrows. The maxima are roughly coincident with the expected location as revealed from the analysis of the mean squared fluctuations in Fig.4 and the inflection points of density profiles. However, their value is far smaller than $2/3$, the expected result for a critical point, and lend further support to our claim of rounded layering transitions.

DENSITY PROFILES FOR SOLID-LIKE MOLECULES

Density profiles for solid-like molecules for a selected range of temperatures are shown in Fig. 6.

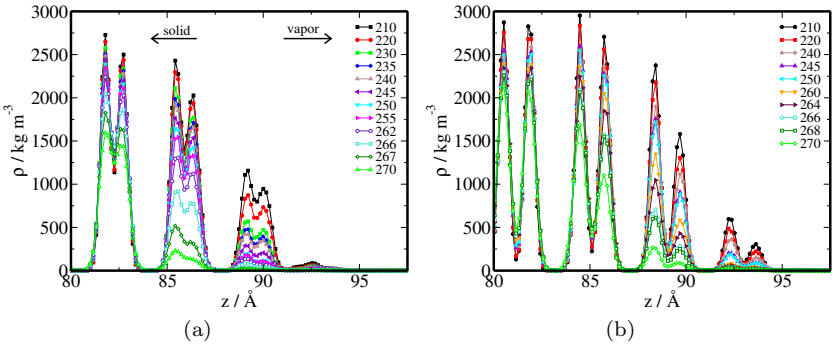

FIG. 6. Density profiles for solid-like molecules as a function of temperature. (a) Basal (b) Prism planes.

PARAMETERS FOR THE FIT TO THE INTERFACE POTENTIAL

The coefficients of the fit for the interfacial potential form given in Eq. (2) in the main text are displayed in Table II.

face	fit	$A_1/J\,m^{-2}$	$A_2/J\,m^{-2}$	κ·Å	κ_R ·Å	$k_{z,R}$·Å	θ/rad
Basal	mf	0.1064	0.00100	0.6170	2κ	2.269	10.919
Basal	R	0.1070	0.00161	0.6102	0.429	2.360	10.323
pI	mf	0.0662	0.000148	0.6078	2κ	3.149	7.716
pI	R	0.0701	0.00379	0.6206	0.900	3.144	7.796

TABLE II. Parameters for the fit of simulated disjoining pressures to the model interface potential in Eq. (2) for basal and prism planes. Results for the constrained fit with $2\kappa = \kappa_R$ are also shown.

COMPUTER SIMULATIONS

At low saturation, ice crystals grow as hexagonal prisms, exhibiting two well defined facets. The base of the prism corresponds to the $\{0001\}$ crystal facets, and is also known as the basal facet. The sides of the prism correspond to $\{10\bar{1}0\}$ facets, and are known as the prism facets. For further details on the preparation of the initial configuration, we refer to our previous work, Ref.[39, 41, 44]

Our simulations are carried out with the TIP4P/Ice model [37]. Phase space sampling is performed using Molecular Dynamics with the GROMACS package. Trajectories are evolved using the Leap-frog algorithm, with a time step of 3 fs. Bond and angle constraints are applied using the LINCS algorithm. Trajectories are thermostated in the NVT ensemble using the velocity rescale algorithm [38]. Lennard-Jones interactions are truncated at a distance of 9 Å. Electrostatic interactions are evaluated using Particle Mesh Ewald, with the real space contribution truncated also at 9 Å. The reciprocal space term is evaluated over a total of $80 \times 64 \times 160$ vectors in the x, y, z reciprocal directions, respectively. The charge structure factors were evaluated with a grid spacing of 0.1 nm and a fourth order interpolation scheme. For each temperature, we performed an NpT simulation at 1 bar to obtain the corresponding equilibrium lattice parameters. The NVT simulations that are then employed use equilibrated lattice parameters at that temperature. In order to prepare roughly square surfaces, we build a unit supercell of size $(2 \times a) \times b \times c$, with a, b and c, the unit cell parameters of a pseudo-orthorhombic cell of 8 molecules. Simulations are performed for two system sizes, a large system size, consisting of $8 \times 8 \times 5$ and a smaller one with $4 \times 4 \times 5$ unit supercell with 16 molecules each. More detailed information on the simulations may be found in our previous work [39, 41, 44].

Details of the system sizes studied may be found in Tables III and IV. Results for the film thickness may be found in Tables V and VI. Further details of the simulations may be found in [41].

ORDER PARAMETER

In our study, we need to distinguish solid-like from liquid-like molecular environments in order to determine the premelting layer thickness and to locate the ice/water surface. For each water molecule, we perform a neighbor analysis and determine the $\bar{q}_6$ parameter, which is known to distinguish well solid and liquid molecules in bulk environments [42]. All water molecules with $\bar{q}_6$ larger than a threshold value, $\bar{q}_6^*$, are classified as solid-like, while molecules with smaller $\bar{q}_6$ parameter are classified as liquid-like. In order to calculate the threshold value, we perform simulations of the bulk solid and liquid phases. From the distribution of $\bar{q}_6$ in each phase, we determine the value of $\bar{q}_6^*$ which produces the least amount of mislabeling. The threshold value is $\bar{q}_6^* \approx 0.35$ in the neighborhood of the triple point, but depends slightly on temperature. We refer to our recent work for further details and explicit results for the dependence of $\bar{q}_6^*$ on temperature [41].

An interesting alternative to the $\bar{q}_6$ parameter is the CHILL+ algorithm, which has been devised explicitly to discriminate solid-like environments different from hexagonal ice Ih [43]. In particular, the CHILL+ algorithm allows one to identify other ice crystal allotropes such as ice Ic, clathrate ice and interfacial ice Ih. In our previous work [41], we have shown that the $\bar{q}_6$ parameter essentially lumps all of these forms into the disordered liquid-like category. Therefore, our choice of order parameter essentially distinguishes the bulk ice Ih template from all other ice environments. The conventional application of CHILL+ is to label solid and liquid-like molecules in the the opposite extreme, i.e. to have the intermediate forms ice Ic, chlathrate ice and interfacial ice Ih lumped into the solid-like category, and have the liquid-like category for all remaining disordered forms. Fig. 7 display premelting film thicknesses as dictated by either of these two prescriptions. Starting from a temperature of about $T = 240$ K, we find that either deffinitions differ essentially by a constant offset. Below this temperature, on the other hand, we find that both parameters are

very similar. It follows that the first transition found in our work corresponds to an increase of undercoordinated ice forms. Surprisingly, both the $\bar{q}_6$ and CHILL+ recipes yield a close to monolayer thick disordered liquid layer at temperatures as low as 210 K. A detailed analysis of surface ice structure and coordination is left for future work.

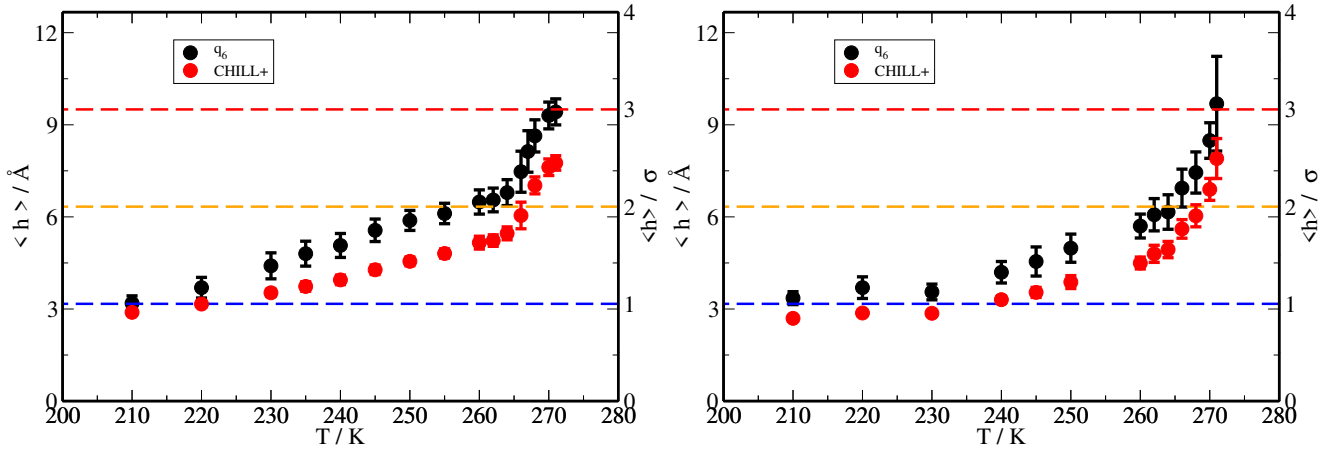

FIG. 7. Premelting layer thickness measured using the $\bar{q}_6$ parameter as in this work (black), and with the CHILL+ parameter (red) for basal (left) and prism (right) facets.

INTRINSIC SURFACES

For each saved snapshot, we calculate the i-f and f-v intrinsic surfaces, meant to describe the local height of the premelting film at each point $\mathbf{x}$ on a reference plane parallel to the interface. First we analyze the local environment of each molecule in order to label them as liquid-like or solid-like with the $\bar{q}_6$ order parameter as described above [42]. For a given point, $\mathbf{x}$, we calculate the i-f surface as the vertical position, $z_{\mathrm{i-f}}(\mathbf{x})$ obtained from the average z position of the four outermost solid-like atoms within one pseudo-orthorhombic unit cell of size $a \times b \times c$ about the point $\mathbf{x}$. Likewise, the f-v surface is calculated from the average z position of the four outermost liquid-like molecules within an area of $3\sigma \times 3\sigma$ about $\mathbf{x}$, with σ the Lennard-Jones range parameter of the TIP4P/Ice model. The procedure is illustrated in Fig. 8.

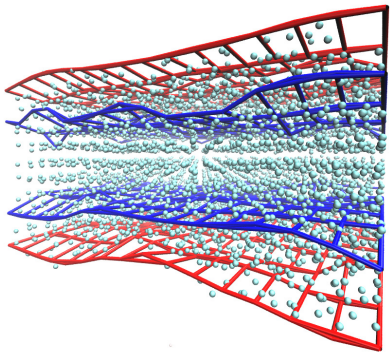

FIG. 8. Sketch showing the i-f and f-v bounding surfaces that we employ to characterize the premelting film. The i-f surface is shown in blue and the f-v surface is shown in red.

SYSTEM SIZES STUDIED

Detailed information on the system sizes studied are described in Tables III and IV.

Temperature / K	$N = 5120$, $L_x \times L_y \times L_z$ / nm	$N = 1280$, $L_x \times L_y \times L_z$ / nm
210	7.24541 × 6.27494 × 15.00000	3.62270 × 3.13747 × 15.00000
220	7.24868 × 6.27776 × 15.00000	3.62434 × 3.13888 × 15.00000
230	7.25247 × 6.28104 × 15.00000	3.62623 × 3.14052 × 15.00000
235	7.25427 × 6.28292 × 15.00000	3.62714 × 3.14146 × 15.00000
240	7.25609 × 6.28412 × 15.00000	3.62804 × 3.14206 × 15.00000
245	7.25780 × 6.28587 × 15.00000	3.62890 × 3.14294 × 15.00000
250	7.25949 × 6.28713 × 15.00000	3.62974 × 3.14356 × 15.00000
255	7.26152 × 6.28888 × 15.00000	3.63076 × 3.14444 × 15.00000
260	7.26350 × 6.29060 × 15.00000	3.63175 × 3.14530 × 15.00000
262	7.26419 × 6.29120 × 15.00000	3.63209 × 3.14560 × 15.00000
264	7.26488 × 6.29181 × 15.00000	3.63244 × 3.14590 × 15.00000
266	7.26558 × 6.29241 × 15.00000	3.63270 × 3.14620 × 15.00000
267	7.26586 × 6.29264 × 15.00000	3.63293 × 3.14632 × 15.00000
268	7.26628 × 6.29302 × 15.00000	3.63314 × 3.14651 × 15.00000
270	7.26698 × 6.29362 × 15.00000	3.63349 × 3.14681 × 15.00000
271	7.26731 × 6.29432 × 15.00000	3.63360 × 3.14716 × 15.00000

TABLE III. Temperature and systems dimensions for the basal interface. The number of unit cells in x, y and z directions are $N_x = 8$, $N_y = 8$ and $N_z = 5$ for the bigger system. The small system has half $(N/2)$ unit cells in the x and y directions and equal number of unit cells along z.

Temperature / K	$N = 5120$, $L_x \times L_y \times L_z$ / nm	$N = 1280$, $L_x \times L_y \times L_z$ / nm
210	7.24528 × 5.89679 × 15.00000	3.62270 × 2.94840 × 15.00000
220	7.24876 × 5.89961 × 15.00000	3.62434 × 2.94980 × 15.00000
230	7.25229 × 5.90249 × 15.00000	3.62623 × 2.95124 × 15.00000
240	7.25604 × 5.90554 × 15.00000	3.62804 × 2.95277 × 15.00000
245	7.25780 × 5.90697 × 15.00000	3.62890 × 2.95348 × 15.00000
250	7.25957 × 5.90841 × 15.00000	3.62974 × 2.95420 × 15.00000
260	7.26329 × 5.91143 × 15.00000	3.63175 × 2.95571 × 15.00000
262	7.26405 × 5.91205 × 15.00000	3.63209 × 2.95602 × 15.00000
264	7.26480 × 5.91267 × 15.00000	3.63244 × 2.95633 × 15.00000
266	7.26556 × 5.91328 × 15.00000	3.63270 × 2.95664 × 15.00000
268	7.26631 × 5.91389 × 15.00000	3.63314 × 2.95694 × 15.00000
270	7.26707 × 5.91452 × 15.00000	3.63349 × 2.95726 × 15.00000
271	7.26729 × 5.91470 × 15.00000	3.63360 × 2.95735 × 15.00000

TABLE IV. Temperature and systems dimensions for the prism face. The number of unit cells is as for the basal face listed in the caption of Table III

FILM THICKNESS FOR TWO DIFFERENT SYSTEM SIZES

The film thicknesses displayed in Figures in the text are shown in tabulated form in Tables V and VI.

Temperature / K	$\langle h \rangle$ / Å(Area = 1)	$\langle h \rangle$ / Å(Area = $\frac{1}{4}$)
210	3.18	3.29
220	3.69	4.23
230	4.40	3.46
235	4.80	5.10
240	5.07	5.17
245	5.56	5.66
250	5.88	5.90
255	6.11	6.12
260	6.48	6.83
262	6.55	6.69
264	6.79	7.80
266	7.47	8.18
267	8.13	8.63
268	8.63	9.18
270	9.30	9.32
271	9.42	9.19

TABLE V. Thickness as a function of temperature for the basal face and the two systems simulated.

Temperature / K	$\langle h \rangle$ / Å(Area = 1)	$\langle h \rangle$ / Å(Area = $\frac{1}{4}$)
210	3.35	3.08
220	3.69	3.15
230	3.55	3.60
240	4.20	4.26
245	4.55	4.87
250	4.98	4.94
260	5.70	5.73
262	6.07	5.70
264	6.16	5.88
266	6.94	6.26
268	7.44	7.44
270	8.49	7.55
271	9.69	8.34

TABLE VI. Thickness as a function of temperature for the prism face and the two systems simulated.